Energy Equip. Sys./ Vol. 6/No. 3/Sep. 2018/ 293-303

ENERGY EQUIPSYS

Energy Equipment and Systems

http://energyequipsys.ut.ac.ir
www.energyequipsys.com

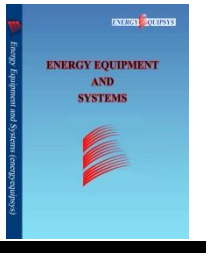

Improving the natural convective heat transfer of a rectangular heatsink using superhydrophobic walls: A numerical approach

Author

Milad Shakeri Bonab [a]
Abolfazl Anarjani Khosroshahi [a]
Mehdi Ashjaee [a]
Seyed Farshid Chini [a*]

[a] Department of Mechanical Engineering, College of Engineering, University of Tehran, Tehran, Iran

Article history:

Received : 01 December 2017
Accepted : 28 May 2018

ABSTRACT

The effect of utilizing superhydrophobic walls on improving the convective heat transfer in a rectangular heatsink has been studied numerically in this paper. The vertical walls were kept at isothermal hot-and-cold temperatures and horizontal walls were insulated. The boundary condition on the walls was: no-slip for regular, and slip (with slip length of 500 μm) for superhydrophobic walls. By changing the heatsink aspect ratio (AR, height/width) from 0.1 to 10, it was observed that regardless of the wall slip, the optimum AR is 1, i.e. square enclosure. For a square heatsink, using the nanofluid with φ = 3% could enhance the heat transfer (quantified by Nusselt number) by up to 9.8%. For the same enclosure filled with pure water, applying superhydrophobic horizontal walls could increase the heat transfer by 4.45%. The joint effect of using superhydrophobic walls and nano-particles enhanced the heat transfer by up to 14.75%. The results of this paper may open a new avenue for high performance cooling systems.

Keywords: Natural Convection, Heatsink, Local Cooling, Nanofluid, Superhydrophobic, Slip Length.

1. Introduction

High performance cooling is one of the essential requirements in many industries, e.g. furnace engineering [1], non-Newtonian chemical processes [2,3], solar energy storages [4], chemical vapor depositions, [5] and surfaces under a magnetic field [6,7]. In order to save energy, instead of cooling the whole environment, it is feasible to cool the desired locations, i.e., local cooling. One of the local cooling techniques is – applying convective heat transfer. Convective heat transfer is widely used in cooling datacenters and microprocessors [8]. As processors become smaller, heat dissipation becomes challenging [9]. As such, there is always a need to enhance the heat transfer. Earlier processor coolers used forced air to dissipate the heat [10]. Thermal conductivity of liquids is generally greater than gases. Therefore, by using liquid, the fans can be operated at lower speeds and creating less noise, consequently. As such, the next generations used liquid instead of gas.

Khanafer et al. [15] numerically proved that utilization of nanofluids (fluids with suspended metallic or non-metallic nano-particles) can enhance the buoyancy-driven heat transfer inside a two-dimensional enclosure heat sink. To explain the mechanism, different

[*] Corresponding author: Seyed Farshid Chini
Department of Mechanical Engineering, College of Engineering, University of Tehran, Tehran, Iran
Email: chini@ut.ac.ir

explanations are provided in the literature, e.g., increasing surface area, better interaction and collision between particles, and higher irregular and random movement of particles [11]. For numerical models, it should be noted that adding nano-particles in the base liquid increases the effective thermal conductivity (K_{nf}) as well as the effective viscosity (μ_{nf}). Hamilton and Crosser [12] proposed a relation for K_{nf} of a mixture of liquid and solid where the thermal conductivity of solid particles was at least 100 times greater than the liquid. The relation was later simplified for spherical solid particles [13]. The simplified relation [13] is applied to nanofluids [14,15]. For μ_{nf}, Einstein [16] developed a relation for an infinitely dilute suspension of small spheres in a liquid. The relation was modified and applied to nanofluids by Brinkman [17]. Earlier numerical studies were unable to show the increase in heat transfer by increasing the nanofluid volume fraction (φ), e.g. [18]. This is because they used the Nusselt number (Nu) to compare the heat transfer rates. Using Nu can be misleading, as nano-particles increase both the fluid convection and conduction simultaneously. For that, in recent studies (e.g. [15] [19] [20]), the Nu is calculated using thermal conductivity of the base liquid and not the K_{nf}. With this adjustment, numerical models can follow the experiments, i.e., increasing trend of heat transfer by increasing the φ. Another adjustment for numerical results is as follows: experimentally there is an upper limit for φ and beyond that the numerical results are not meaningful. As shown [21], for φ values larger than 3%, increasing the φ may deteriorate the natural-convective heat transfer. In this paper, we limit our studies to φ values smaller than 3%.

For smaller enclosures, surface forces become dominant (compared to volume forces). Therefore, sheer stress at the wall can be an effective parameter in heat transfer of small heatsinks [22] [23]. Adding a small amount of drag-reducing polymer or surfactant additives may significantly reduce the wall friction [23]. However, the drawback is that nanofluids may not be compatible with the applied polymers. One of the novel methods for reducing friction drag is using superhydrophobic (SHP) surfaces [24]. Superhydrophobic surfaces have contact angles greater than 150° (see Fig.1) and contact angle hysteresis (CAH) less than 5° [25]. [CAH is the difference between advancing and receding contact angles (maximum and minimum possible contact angles on a surface)]. These surfaces are inspired from nature, e.g. lotus leaves. Some of the interesting properties of SHP surfaces are self-cleaning [26], corrosion-resisting, drag-reducing [27], and anti-icing [28]. To manufacture SHP surfaces, the surface should be rough in micro and nano scale and have low surface energy.

Fluids on regular surfaces are motionless, i.e., no-slip condition. Fluids on superhydrophobic surfaces have slip velocity (u_{slip}, see Eq.(1)). The velocity profiles are shown for both conditions in Fig 2. To quantify the slip velocity, Navier's slip length (β_{slip}) is used [24]:

$$u_{slip} = \beta_{slip} \left.\frac{du}{dy}\right|_{wall} \quad (1)$$

The β_{slip} on regular surfaces is a few nanometers. On superhydrophobic surfaces, β_{slip} is in the order of hundreds of micrometers, [24] and can be as large as 500 μm. The slip length depends on some parameters such as height and width of pillars and ridges. In this paper, the value of β_{slip} for regular and superhydrophobic surfaces are assumed to be 0 and 500 μm, respectively.

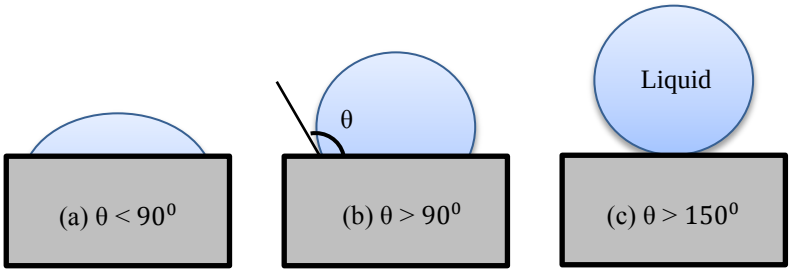

Fig.1. Water drop on a (a) hydrophilic, (b) hydrophobic and (c) superhydrophobic surface is shown. Contact angle is the angle between tangent to the drop interface and substarte at the contact line and measured from inside the liquid

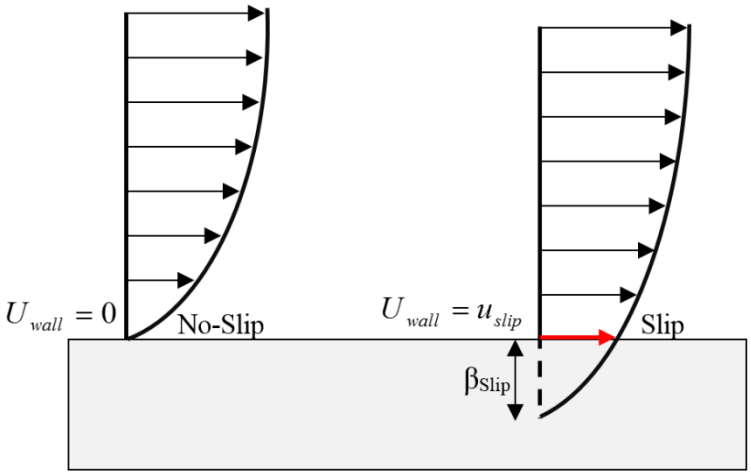

Fig.2. Schematic of no-slip and slip velocity profiles on a solid surface is shown. The slip length (β_{slip}) is found by extrapolating the velocity profile

The purpose of this study is - to numerically investigate the potential of using SHP walls, and their effect on increasing the heat transfer in a heatsink. Then, the joint effect of using SHP walls and Fe_3O_4/water nanofluid was studied. The heatsink model is a 2D rectangular enclosure with a height H and width W (as shown in Fig3). The two vertical walls are isothermal and horizontal walls are insulated. The left vertical wall is heated at a high temperature (T_H) and the right vertical wall is at a lower temperature (T_L). Heat transfer performance of the heatsink is investigated by changing different pertinent parameters in the various states.

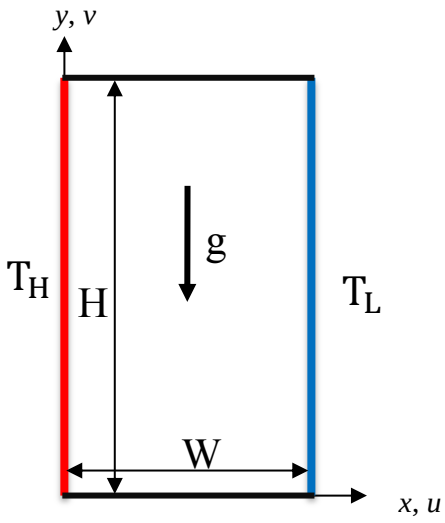

Fig.3. Schematic of the rectangular heatsink is shown. Hot and cold walls are shown with TH and TL, accordingly

2.Methodology

To solve the governing equations, the following assumptions [15], numerical scheme, and algorithm are made: nanofluid is incompressible, Newtonian, and homogeneous. The homogeneity means that nanoparticles and base liquid do not have any temperature and velocity difference. In other words, they are in thermal and momentum equilibrium. The Ra (ratio of buoyancy force to heat diffusion) changes from 10^3 to 10^6. So, the flow is laminar (i.e. Ra<10^9). The value of φ is 3% for nano-fluid and zero for pure water. The following geometrical aspect ratio (AR, H/W) values are tested: 0.1, 0.25, 0.5, and from 1 to 10 (with the step size of 1). The SIMPLE algorithm is used for pressure-velocity coupling. In addition, Finite Volume Scheme has been chosen to discretize the governing equation and QUICK scheme approximation is selected for the advection term. Central differencing with second order accuracy is used for discretizing the diffusion terms. Radiation heat transfer is not considered and gravity acts in *y* direction. All thermo-physical properties of nanofluids are assumed constant, except for density variations which changes with temperature based on Boussinesq approximation. The Boussinesq approximation is valid when variation in the fluid density is small. The solver stops the iterations when the results convergence and discrepancy between the last two iterations was less than 10^{-6}. Properties of the nanofluids are determined based on the models summarized in Table 1.

Thermo-physical properties of the base liquid and nano-particle are listed in Table 2.

Table 1. Formulation of the nanofluid properties based on the applied model

Nanofluid property	Applied model
Heat capacitance [14]	$(\rho C_p)_{nf} = (1-\varphi)(\rho C_p)_f + \varphi(\rho C_p)_p$
Dynamic viscosity [17]	$\mu_{nf} = \mu_f \frac{1}{(1-\varphi)^{2.5}}$
Thermal conductivity [13]	$K_{nf} = K_f \left[\frac{K_p + 2K_f - 2\varphi(K_f - K_p)}{K_p + 2K_f + 2\varphi(K_f - K_p)}\right]$
Thermal expansion [15]	$\frac{\beta_{nf}}{\beta_f} = \left[\frac{1}{1+\frac{(1-\varphi)}{\varphi}\frac{\rho_f}{\rho_p}}\frac{\beta_p}{\beta_f} + \frac{1}{1+\frac{\varphi}{1-\varphi}\frac{\rho_p}{\rho_f}}\right]$

Table 2. Thermo-physical properties of used materials [29] at 20oC

	ρ $[kg/m^3]$	C_p $[J/kgK]$	K $[W/mK]$	μ $[Ns/m^2]$	β $[1/K]$
Pure Water	998.2	4182	0.6	0.001003	2.0661×10^{-4}
Nanoparticle (Fe3O4)	4950	640	7	N/A	1.041×10^{-5}

- Governing equations:

Governing equations for natural convection are continuity, momentum and energy equations. The flow is assumed laminar, 2D, steady-state, and incompressible with Boussinesq approximation [30].

The continuity equation for incompressible fluid in 2D is:

$$\frac{\partial u}{\partial x} + \frac{\partial v}{\partial y} = 0 \tag{2}$$

where x and y are main Cartesian coordinate variables; and u and v are velocity component in x and y direction, respectively.

The x and y momentum equation for incompressible fluid in 2D are:

$$u\frac{\partial u}{\partial x} + v\frac{\partial u}{\partial y} = -\frac{1}{\rho}\frac{\partial p}{\partial x} + \frac{\mu}{\rho}\left(\frac{\partial^2 u}{\partial x^2} + \frac{\partial^2 u}{\partial y^2}\right) \tag{3}$$

$$u\frac{\partial v}{\partial x} + v\frac{\partial v}{\partial y} = -\frac{1}{\rho}\frac{\partial p}{\partial y} + \frac{\mu}{\rho}\left(\frac{\partial^2 v}{\partial x^2} + \frac{\partial^2 v}{\partial y^2}\right) + g\beta(T - T_0) \tag{4}$$

where ρ is density, p is pressure, μ is dynamic viscosity, g is the gravity constant, β is thermal expansion coefficient (see Table 2), T is temperature, and T_0 is reference temperature.

The energy equation for incompressible fluid in 2D is:

$$u\frac{\partial T}{\partial x} + v\frac{\partial T}{\partial y} = \alpha\left(\frac{\partial^2 T}{\partial x^2} + \frac{\partial^2 T}{\partial y^2}\right) \tag{5}$$

where α is thermal diffusivity of fluid. The non-dimensional form of continuity, momentum, and energy equations are:

$$\frac{\partial U}{\partial X} + \frac{\partial V}{\partial Y} = 0 \tag{6}$$

$$U\frac{\partial U}{\partial X} + V\frac{\partial U}{\partial Y} = -\frac{\partial P}{\partial X} + Pr\left(\frac{\partial^2 U}{\partial X^2} + \frac{\partial^2 U}{\partial Y^2}\right) \tag{7}$$

$$U\frac{\partial V}{\partial X} + V\frac{\partial V}{\partial Y} = -\frac{\partial P}{\partial Y} + Pr\left(\frac{\partial^2 V}{\partial X^2} + \frac{\partial^2 V}{\partial Y^2}\right) + RaPr\Theta \tag{8}$$

$$U\frac{\partial \theta}{\partial X} + V\frac{\partial \theta}{\partial Y} = \frac{\partial^2 T}{\partial X^2} + \frac{\partial^2 T}{\partial Y^2} \tag{9}$$

where the non-dimensional variables are given in Table 3.

2.1.Mesh Sensitivity Analysis

For showing the mesh sensitivity and choosing the most appropriate mesh, different mesh sizes were examined (from 10 to 300) for air in a square enclosure (i.e. AR = 1), where Ra was 10^6. Because the temperature gradient near the walls of the enclosure is higher than in other areas, smaller grids are needed around the walls for careful calculations. Figure 4 shows the boundary layer type of mesh used in this study. The Nu number on the hot wall of the heatsink shows that a mesh of 150 is appropriate and enough (Fig. 5). For larger and

smaller enclosures, the mesh size is scaled based on the 150 × 150 grid for AR = 1.

2.2.Validation

The validation of our numerical results was performed only for the cases that the walls were regular (i.e., no-slip condition). The reason is that based on our knowledge, the literature models have not studied the effect of superhydrophobic surfaces for this problem, e.g. [15, 31]. As seen in Table 3, the results of the present work is within 1% of other numerical results and within 10% of the analytical solution in [32].

Moreover, for accurate validation and reliability of our numerical code, the velocity profile in the *y*-direction (Fig. 6a) and the temperature profile (Fig. 6b) along the horizontal imaginary line at the midsection of the heatsink were obtained. These profiles were compared with the results of previous numerical studies [15] for air. It is evident from the comparison that our results are in agreement with previous studies for various Ra numbers.

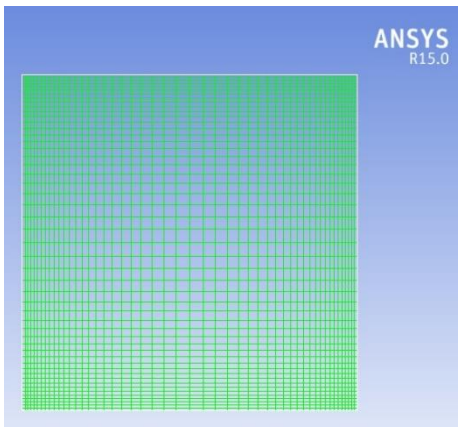

Fig. 4. Boundary layer type of mesh with smaller grids around the walls

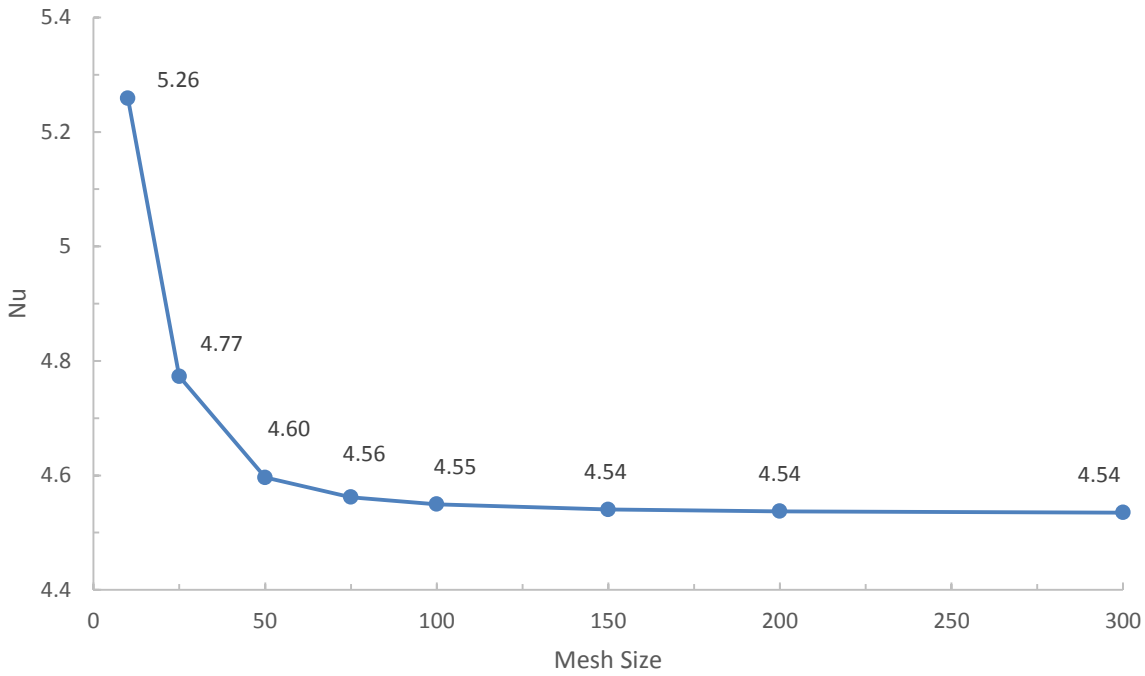

Fig. 5. The value of Nu number on the hot wall of the heatsink is shown for different mesh sizes. It is shown that a mesh size of 150 is appropriate. The solid line is a guide to the eye

Table 3. Comparison of average Nu number with previous works for different Ra values (Pr = 0.7, AR = 1).

Ra	Present work	Khanafer et al. [15]	De Vahl Davis [31]	Incropera [32]
10^3	1.117	1.118	1.118	1.245
10^4	2.246	2.245	2.243	2.428
10^5	4.557	4.522	4.519	4.734
10^6	8.865	8.826	8.799	9.232

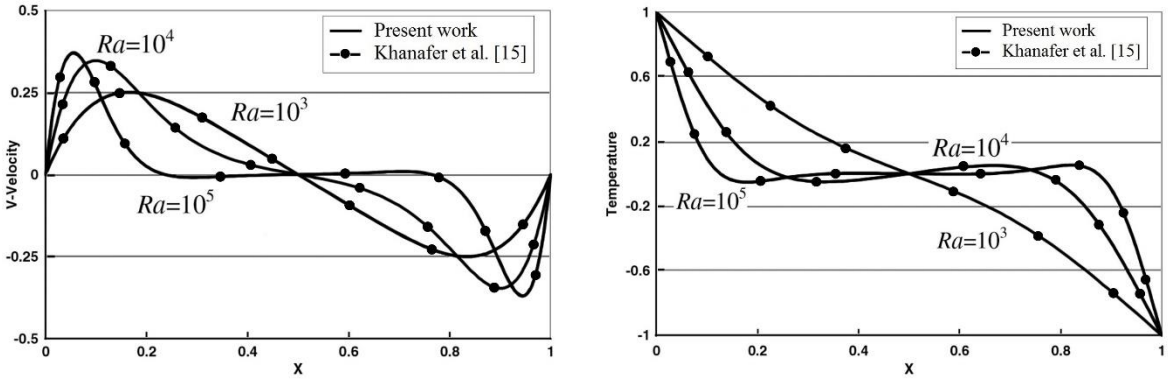

Fig. 6. (a) The velocity profile in the y-direction, and (b) the temprature profile, along the horizontal midsection of the heatsink are shown for different Ra numbers. Fluid is air and AR = 1. It is shown that present work (solid line) and results of [15] (circles) overlap

For validating the results at different AR values, the relation in [32] was used; see

Table 4. Pure water was used for this comparison. Regarding Table 5, it should be noted that in [32] there was no relation for calculating the Nu where AR < 1. As the results depict, the error decreases with increasing AR, due to better fluid flow and heat transfer for vertically heated surfaces.

3.Result and Discussions

By changing the AR value, as shown in Fig. 7, the optimum rectangular enclosure to maximize the heat transfer is a square, i.e. AR = 1. To explain that the AR = 1 is an optimum geometry, the velocity contours at three different AR values are shown in Fig. 7. As shown, for AR= 1, more regular spinal fluid flow is made in enclosure and close to the walls, average magnitude of velocity is larger than that at other AR values. For large AR values, the hot and cold walls become close and the heat transfer mechanism is mainly conduction. For small AR values, convection is the dominant heat transfer mechanism. However, for very small AR values, the hot and cold walls are further apart and circulation is hindered. Therefore, there is an optimum AR value at which the heat transfer is at its maximum, see Fig. 7.

Table 4. The value of Nu in the present study is compared with the value found using the relation in [32] at different AR values. Fluid is pure water and Ra = 10^6

AR	Nu	Nu [32]	Error (%)
1	9.274	9.811	5.785
2	8.366	8.785	5.011
3	7.715	7.938	2.884
4	7.250	7.387	1.898
5	6.895	6.986	1.324
6	6.612	6.675	0.950
7	6.379	6.423	0.691
8	6.181	6.212	0.502
9	6.010	6.032	0.362
10	5.860	5.875	0.256

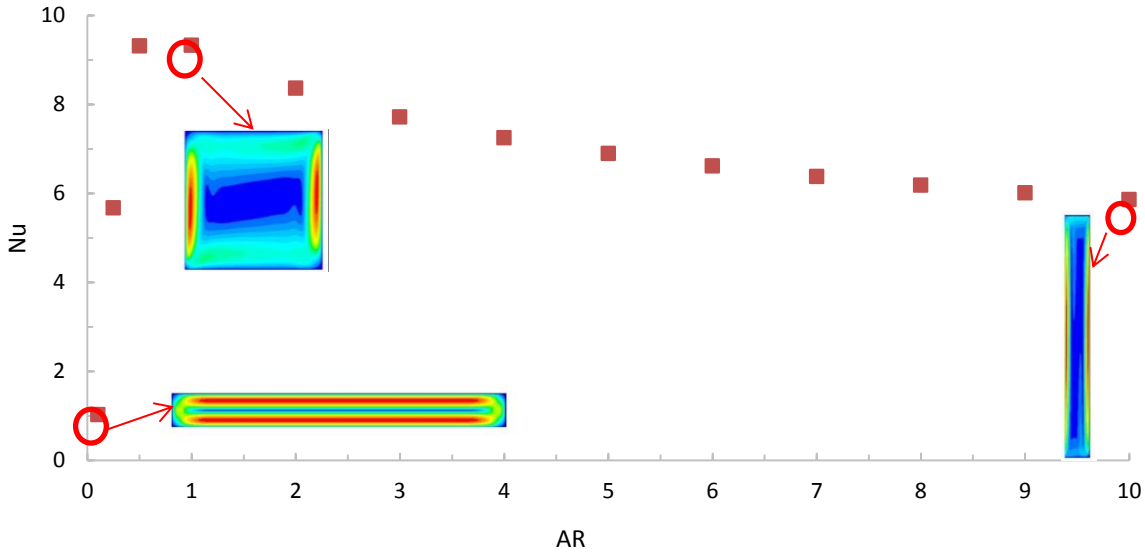

Fig. 7. Comparison of Nu number at different AR values (Ra = 10^6). The velocity contours at AR values of 0.1, 1 and 10 are shown

As explained above, the square enclosure (AR = 1) is optimum geometry and will be used in the rest of this paper. The effect of using nanofluid and superhydrophobic surfaces becomes more observable at larger Ra numbers (larger Ra value is equivalent to larger convective heat transfer). Ra = 106 is used in this study to make sure that the flow remains laminar. It should be noted that this Ra number is roughly equivalent to the Ra value of a square enclosure with the side length of 2 cm and temperature difference of 10oC filled with pure water.

To further increase the heat transfer, the effect of adding the nanoparticles was studied. As shown in Table 5, using nanofluid with φ = 3% results in 9.8% increase in heat transfer of pure water in an enclosure with AR = 1 and Ra = 10^6.

To investigate the effect of superhydrophobic walls on heat transfer, a square enclosure filled with pure water was studied. Slip wall boundary condition (according to Eq. (1)) was applied on top and bottom walls. It is worth noting that when the top and bottom walls are insulated, no temperature jump occurs. The value of Nu number was calculated on the hot and cold (i.e. left and right) walls. Results were compared with the case that all the four walls were regular (no-slip condition walls) and presented in Figs.8 and 9. It was found that applying slip boundary condition (or using SHP walls) for the top or bottom walls have approximately same results, i.e. 2.25% ($\frac{9.483-9.274}{9.274} \times 100\%$) increase in the heat transfer. Using slip boundary condition for both top and bottom walls jointly results in 4.45% ($\frac{9.687-9.274}{9.274} \times 100\%$) increase in the heat transfer. So, it is

suggested to apply superhydrophobic walls only on the two top and bottom walls.

Table 5. Comparison of Nu number for pure water and nanofluid (Ra = 10^6, and AR = 1)

Working fluid	Nu number	Increase (%)
Pure water	9.274	0
φ = 1%	9.568	3.2%
φ = 2%	9.871	6.4%
φ = 3%	10.185	9.8%

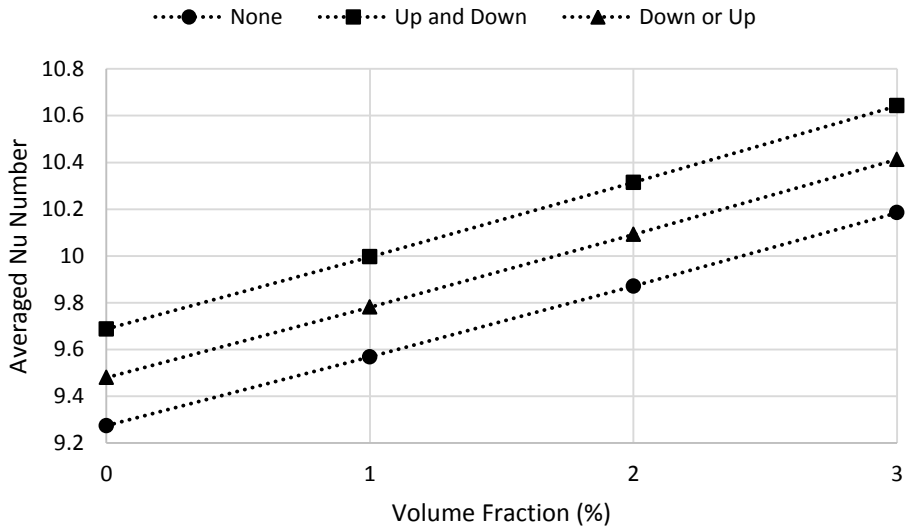

Fig.8. Average Nu number at different φ for various walls condition (Ra = 10^6, AR = 1)

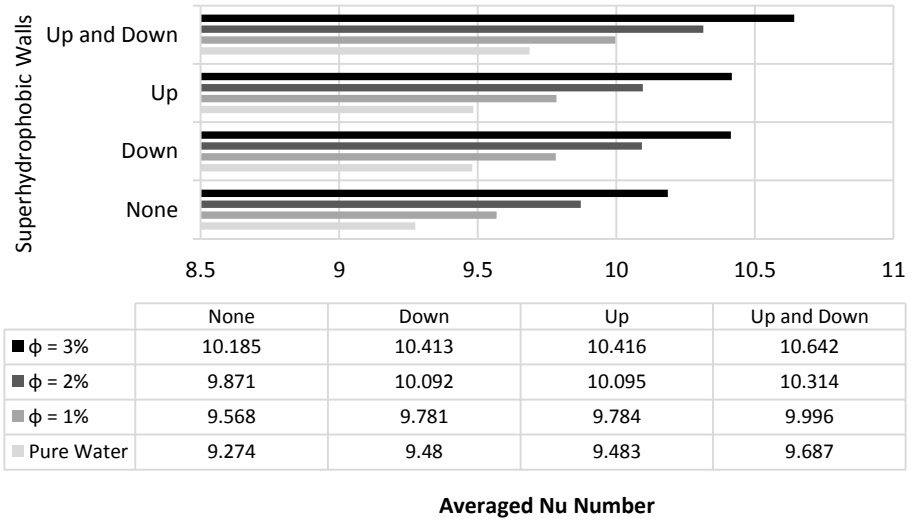

	None	Down	Up	Up and Down
ϕ = 3%	10.185	10.413	10.416	10.642
ϕ = 2%	9.871	10.092	10.095	10.314
ϕ = 1%	9.568	9.781	9.784	9.996
Pure Water	9.274	9.48	9.483	9.687

Fig.9. Comparison of average Nu number for various SHP walls at different φ (Ra = 10^6, AR = 1)

To better understand the joint effect of applying superhydrophobic surfaces and nanofluids, we changed the φ from zero to 3% and applied slip conditions on the walls. As

shown in Table 6, for a regular enclosure (no-slip) with Ra = 10^6 and AR = 1, nanofluid, by itself, increases the heat transfer by almost 9.8% ($\frac{10.185-9.274}{9.274} \times 100\%$). The combined effect of using superhydrophobic walls (top and bottom walls) and nanofluids ($\varphi = 3\%$) may enhance the heat transfer by up to 14.75% ($\frac{10.642-9.274}{9.274} \times 100\%$).

To better understand and explain the effect of SHP walls, the velocity contour inside the enclosure is shown in Fig. 10. As depicted, by making the top and bottom walls superhydrophobic, the streamlines tend to up and down walls and it means that the velocity on these walls is not zero and the streamlines spin better in the clockwise direction.

The streamline spin is better illustrated in Fig 11, where the isotherm contours are compared. As depicted in Fig 11, by applying SHP walls, isotherm lines spin clockwise. The clockwise rotation is consistent with the direction of natural convection.

These findings open up entirely new avenues for high performance cooling devices and micro-processor cooling technologies.

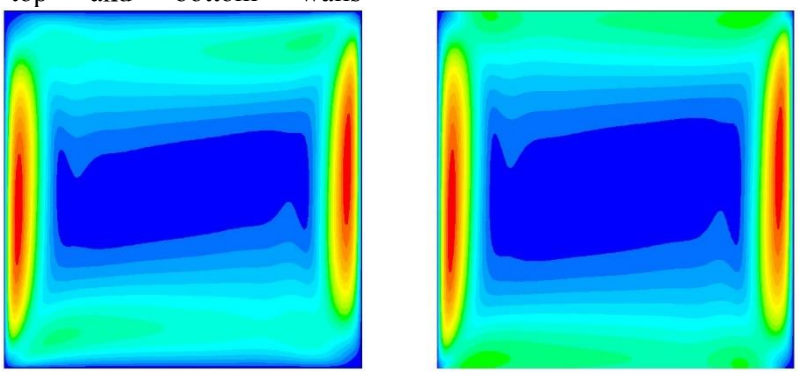

(a) (b)

Fig. 10. Contours of velocity magnitude and Streamline contours for (a) regular walls, (b) up and down SHP walls are shown where Ra = 10^6

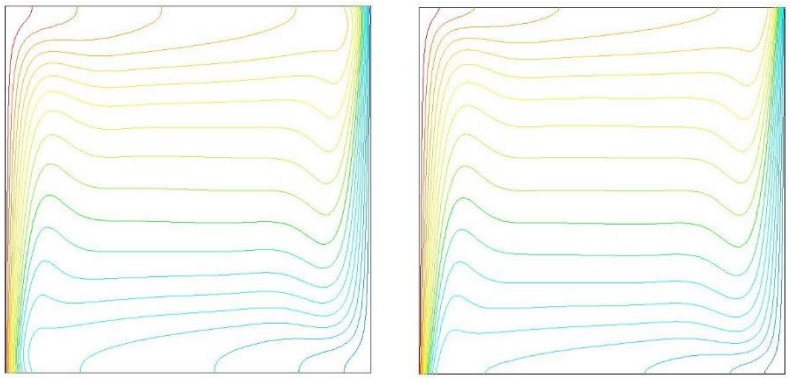

(a) (b)

Fig 11. Isotherm contours for (a) regular walls, (b) up and down SHP walls. (Ra = 10^6)

4.Conclusion

In this research, the potential of using superhydrophobic (SHP) walls for enhancing the natural heat transfer in a rectangular heatsink filled with nanofluid was studied numerically. The slip length for superhydrophobic surfaces was assumed as 500 μm; **φ** varied from 0 to 3%; AR changed from 0.1 to 10; and Ra was consistent at 106, to ensure the flow stays laminar. The vertical walls were kept at isothermal hot and cold temperatures, and the horizontal walls were insulated. The most important results are as follows:

- The optimum rectangular geometry for the heatsink is a square. When the two walls are close to each other, convection becomes negligible and the heat transfer decreases.
- The presence of 3% Fe3O4 nanoparticles inside the base liquid increases the Nu

number by up to 9.8%. By adding nanofluid, both the conduction as well as convection heat transfer increase.

- Using SHP horizontal walls can improve the heat transfer for pure water by up to 4.45%. By applying SHP walls, the fluid inside the heatsink flows on the walls and this results in increase in convection.
- The joint effect of using superhydrophobic walls and nanofluids may enhance the heat transfer by 14.75%.
- At larger Ra numbers, the effect of applying superhydrophobic walls and nanofluids becomes more pronounced. At a larger Ra number, the order of magnitude of velocity is larger, and this larger velocity results in larger velocity gradient on the wall which results in higher slip velocity on superhydrophobic walls.

References

[1] Lim K.O., Lee K.S., Song T.H., Primary and Secondary Instabilities in a Glass-Melting Surface, Numerical Heat Transfer, Part A, Applications (2010).

[2] Patil P. M., Kulkarni P. S., Effects of Chemical Reaction on Free Convective Flow of a Polar Fluid through a Porous Medium in the Presence of Internal Heat Generation, The International Journal of Thermal Sciences (2008) 47(8):1043–1054.

[3] Lamsaadi M., Naïmi M., Hasnaoui M., Mamou M., Natural Convection in a Vertical Rectangular Cavity Filled with a Non-Newtonian Power Law Fluid and Subjected to a Horizontal Temperature Gradient, Numerical Heat Transfer, Part A, Applications (2006).

[4] Singh S., Sharif M. A. R., Mixed Convective Cooling of a Rectangular Cavity with Inlet and Exit Openings on Differentially Heated Side Walls, Numerical Heat Transfer: Part A Applications (2003) 44(3):233–253.

[5] Iwanik P. O., Chiu W. K. S., Temperature Distribution of an Optical Fiber Traversing through a Chemical Vapor Deposition Reactor, Numerical Heat Transfer: Part A Applications (2003) 43(3):221–237.

[6] Saha L. K., Hossain M. A., Gorla R. S. R., Effect of Hall Current on the MHD Laminar Natural Convection Flow from a Vertical Permeable Flat Plate with Uniform Surface Temperature, Journal of Thermal Science (2007) 46(8): 790–801.

[7] Yan Y. Y., Zhang H. B., Hull J. B., Nmrical Modeling of Electrohydrodynamic (EHD) Effect on Natural Convection in an Enclosure, Numerical Heat Transfer: Part A Applications (2004) 46(5): 453–471.

[8] Incropera F. P., Convection Heat Transfer in Electronic Equipment Cooling, The Journal of Heat Transfer (1988) 110(4b):1097.

[9] Go J. S., Kim S. J., Lim G., Yun H., Lee J., Song I., Pak Y. E., Heat Transfer Enhancement Using Flow-Induced Vibration of a Microfin Array, Sensors and Actuators A: Physical (2001) 90(3):232–239.

[10] Air Cooling Technology for Electronic Equipment. CRC Press (1996).

[11] Wang X. Q., Mujumdar A. S., Heat Transfer Characteristics of NanoFluids: A Review, The International Journal of Thermal Sciences (2007) 46 (1): 1–19.

[12] Hamilton R. L., Crosser O. K., Thermal Conductivity of Heterogeneous Two-Component Systems (2002).

[13] Wasp E.J., Kenny J.P., Gandhi R.L., Solid–Liquid Slurry Pipeline Transportation, Bulk Material Handling Trans Tech Publications (1999).

[14] Xuan Y., Roetzel W., Conceptions for Heat Transfer Correlation of Nanofluids, International Journal of Heat and Mass Transfer (2000) 43(19): 3701–3707.

[15] Khanafer K., Vafai K., Lightstone M., Buoyancy-Driven Heat Transfer Enhancement in a Two-Dimensional Enclosure Utilizing Nanofluids, International Journal of Heat and Mass Transfer (2003) 46(19): 3639–3653.

[16] Einstein A., Investigations on the Theory of the Brownian Movement. Courier Corporation (1956).

[17] Brinkman H. C., The Viscosity of Concentrated Suspensions and Solutions, The Journal of Chemical Physics (1952) 20 (4): 571.

[18] Hwang K. S., Lee J.-H., Jang S. P., Buoyancy-Driven Heat Transfer of Water-Based Al2O3 Nanofluids in a Rectangular Cavity, International Journal of Heat and Mass Transfer (2007) 50(19–20): 4003–4010.

[19] Fattahi E., Farhadi M., Sedighi K., Nemati H., Lattice Boltzmann Simulation of Natural Convection Heat Transfer in Nanofluids, The International Journal of Thermal Sciences (2012) 52(1): 137–144.

[20] Panitapu B., Reddy K. K. T., Ramesh M., Reddy K. S., Heat Transfer Enhancement in Natural Convection Using Water Based Fe3O4 Nanofluid Inside a Square Cavity. International Conference on Heat Transfer, Fluid Mechanics and Thermodynamics (2014).

[21] Afrand M., Toghraie D., Sina N., Experimental Study on Thermal Conductivity of Water-Based Fe3O4 Nanofluid: Development of a New Correlation and Modeled by Artificial Neural Network, International Communications in Heat and Mass Transfer (2016) 75: 262–269.

[22] Betz A. R., Jenkins J., Kim C.-J., Attinger D., Boiling Heat Transfer on Superhydrophilic, Superhydrophobic, and Superbiphilic Surfaces, International Journal of Heat and Mass Transfer (2013) 57(2): 733–741.

[23] Li F. C., Kawaguchi Y., Yu B., Wei J. J., Hishida K., Experimental Study of Drag-reduction Mechanism for a Dilute Surfactant Solution Flow, International Journal of Heat and Mass Transfer (2008) 51(3–4): 835–843.

[24] Choi C., Kim M., Wettability Effects on Heat Transfer (2010).

[25] McHale G., Shirtcliffe N. J., Newton M. I., Contact-Angle Hysteresis on Super-Hydrophobic Surfaces, Langmuir (2004) 20(23):10146–10149.

[26] Nakajima A., Hashimoto K., Watanabe T., Takai K., Yamauchi G., Fujishima A., Transparent Superhydrophobic Thin Films with Self-Cleaning Properties, Langmuir (2000) 16(17): 7044–7047.

[27] Bhushan P. B., Jung Y. C., Lotus Effect : Surfaces with Roughness- y y Self-Cleaning g Induced Superhydrophobicity , and Low Adhesion Prof Bharat Bhushan Biomimetics- examples from nature.

[28] Zheng S., Li C., Fu Q., Hu W., Xiang T., Wang Q., Du M., Liu X., Chen Z., Development of Stable Superhydrophobic Coatings on Aluminum Surface for Corrosion-Resistant, Self-Cleaning, and Anti-Icing Applications, Materials & Design (2016) 93: 261–270.

[29] Goharkhah M., Ashjaee M., Effect of an Alternating Nonuniform Magnetic Field on Ferrofluid Flow and Heat Transfer in a Channel, The Journal of Magnetism and Magnetic Materials (2014) 362: 80–89.

[30] Xu X., Yu Z., Hu Y., Fan L., Cen K., A Numerical Study of Laminar Natural Convective Heat Transfer Around a Horizontal Cylinder Inside a Concentric Air-Filled Triangular Enclosure, International Journal of Heat and Mass Transfer (2010) 53(1): 345–355.

[31] Sojoudi A., Saha S. C., Xu F., Gu Y. T., Transient Air Flow and Heat Transfer Due to Differential Heating on Inclined Walls and Heat Source Placed on the Bottom Wall in a Partitioned Attic Shaped Space (2016) 113:39–50.

[32] De Vahl Davis G., Natural Convection of Air in a Square Cavity: A Bench Mark Numerical Solution, The International Journal for Numerical Methods in Fluids (1983) 3(3): 249–264.

[33] Incropera F. P., DeWitt D. P., Introduction to Heat Transfer, 6th Edition, New York: J. Wiley (1990).